Optical and Quantum Electronics **21** *(1989) 283–306*

Two-photon absorption and emission dynamics of bulk GaAs

A. PENZKOFER, A. A. BUGAYEV*
Naturwissenschaftliche Fakultät II – Physik, Universität Regensburg, D-8400 Regensburg, FRG

Received 17 July; revised 1 November; accepted 4 November 1988

Bulk n-type GaAs (dopant silicon) is investigated with picosecond pump pulses of a passively mode-locked Nd:glass laser. The two-photon absorption, the spontaneous emission, and the longitudinal amplified spontaneous emission are measured. The experimental results are compared with computer simulations and relevant material parameters are determined.

1. Introduction

The two-photon absorption cross-section of GaAs at the frequency of Nd-lasers has been determined in the past by transmission [1–16], luminescence [17] and photoconductivity measurements [18]. Besides some large values [1, 2, 4, 6–8, 17, 18] the two-photon absorption coefficient was found to be centred around $(3.5 \pm 2) \times 10^{-8}\,\mathrm{cm\,W^{-1}}$ [3, 5, 9–16].

The luminescence of single-photon excited GaAs is reviewed in [19–24]. Stimulated emission of single-photon excited GaAs is reported in [23, 25, 26]. The two-photon excited luminescence of GaAs was studied in [1, 17, 27–29]. The two-photon-induced luminescence was applied to determine the two-photon absorption cross-section [17]. Two-photon-induced laser action [1, 27–29] and amplified spontaneous emission [27] transverse to the excitation pulse have been achieved in bulk GaAs.

In this paper the two-photon absorption and emission dynamics is studied. n-type GaAs crystals are investigated (dopant is silicon, dopant number density $N_{C,EQ} \approx 1.5 \times 10^{17}\,\mathrm{cm^{-3}}$, Hall mobility $\mu_H \approx 4100\,\mathrm{cm^2\,V^{-1}\,s^{-1}}$, sample lengths 2.5 and 0.5 mm). Single picosecond pulses of a passively mode-locked Nd-phosphate glass laser are used in the experiments (pulse duration $\Delta t_L \approx 5\,\mathrm{ps}$). The two-photon absorption coefficient is determined from transmission measurements. The two-photon pumped spontaneous emission and longitudinal amplified spontaneous emission are studied. The measurements are carried out at the temperatures $\theta \approx 295$ and 103 K. The experimental results are compared with computer calculations. The single-photon absorption dynamics of the deep-level EL2 centres of GaAs [30–41] is included.

2. Measurements

2.1. Linear absorption

The linear absorption of the GaAs sample (length $l = 2.5\,\mathrm{mm}$) below the bandgap edge is measured with a conventional spectrometer (Beckman type ACTA MIV) at room

*On leave from: A. F. Ioffe Physico-Technical Institute, Leningrad, USSR.

0306-8919/89 $03.00 + .12

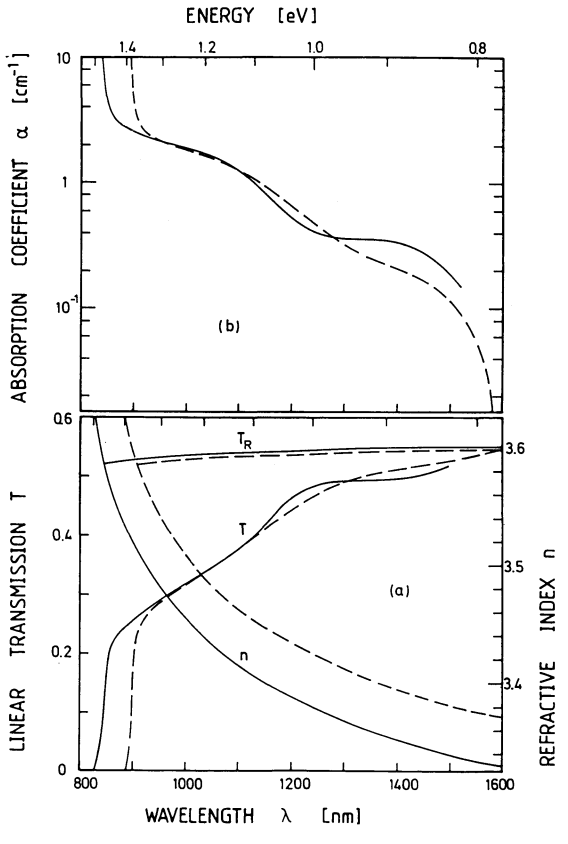

Figure 1 (a) Linear transmission and refractive index [42, 43] of GaAs sample plotted against wavelength. The transmission limit T_R due to the reflection R' is included. (b) Absorption coefficient plotted against wavelength. (——) Temperature $\theta \approx 103$ K; (– – –) $\theta = 295$ K.

temperature (about 22° C) and at low temperature (about 103 K, sample on a cold finger of a liquid-nitrogen cryostat). The transmission curves obtained are shown in Fig. 1a. The transmissions, $T_R = (1 - R')/(1 + R')$ $(R' = (n - 1)^2/(n + 1)^2)$, determined by the refractive index n are included. The refractive index curves are taken from [42, 43].

The absorption coefficient spectra $\alpha(\lambda)$ are determined from the linear transmission data $T(\lambda)$ by an iterative numerical solution of the implicit equation

$$\alpha = (1/l)\{\ln [TR^2 \exp(-\alpha l) + (1 - R)^2] - \ln T\} \tag{1}$$

which is derived from [22, equation 4-32]

$$T = \frac{(1 - R)^2 \exp(-\alpha l)}{1 - R^2 \exp(-2\alpha l)} \tag{2}$$

The reflectance R is given by

$$R = \frac{(n - 1)^2 + \kappa^2}{(n + 1)^2 + \kappa^2} \tag{3}$$

where the extinction coefficient κ is

$$\kappa = \frac{\alpha}{4\pi\tilde{\nu}} = \frac{\alpha\lambda}{4\pi} \tag{4}$$

$\tilde{\nu}$ is the wavenumber and λ is the vacuum wavelength.

The $\alpha(\lambda)$ spectra obtained are shown in Fig. 1b. The absorption below the fundamental edge (energy gap $E_G = 1.425\,\text{eV} = 11\,500\,\text{cm}^{-1} = 871\,\text{nm}$ at 295 K; $E_G = 1.50\,\text{eV} = 12\,090\,\text{cm}^{-1} = 827\,\text{nm}$ at 103 K, see [44, equation 45], is thought to be due to EL2 centres [30–41]. Using an absorption cross-section of $\sigma_I = 1 \times 10^{-16}\,\text{cm}^2$ at $\lambda_L = 1.054\,\mu\text{m}$ [36] an EL2 centre concentration of $N_I \approx 1.6 \times 10^{16}\,\text{cm}^{-3}$ is estimated.

2.2. Non-linear absorption

The experimental set-up for the non-linear transmission measurement and the fluorescence measurement is shown in Fig. 2a. Single pulses of a passively mode-locked Nd-phosphate glass laser were applied ($\Delta t_L \approx 5\,\text{ps}$). The saturable absorber cell SA1 (Kodak dye No. 9860, small-signal transmission 10%) reduced the background energy content. The pump pulse peak intensity was derived from energy transmission measurements through a saturable absorber [45] (cell SA2 filled with Kodak dye No. 9860, small-signal transmission 17.3%, photodetectors PD1 and PD2). The [111] direction of the crystal was normal to the entrance and exit surface (the light propagation direction is parallel to the [111] direction). The energy transmission T_E was measured with the detectors PD1 and PD3. The beam profile of the transmitted laser pulses was monitored with a linear diode array DA. The photomultiplier PM1 registered the fluorescence signal in the forward direction. The monochromator MO together with the photomultiplier PM2 resolved the fluorescence spectrum.

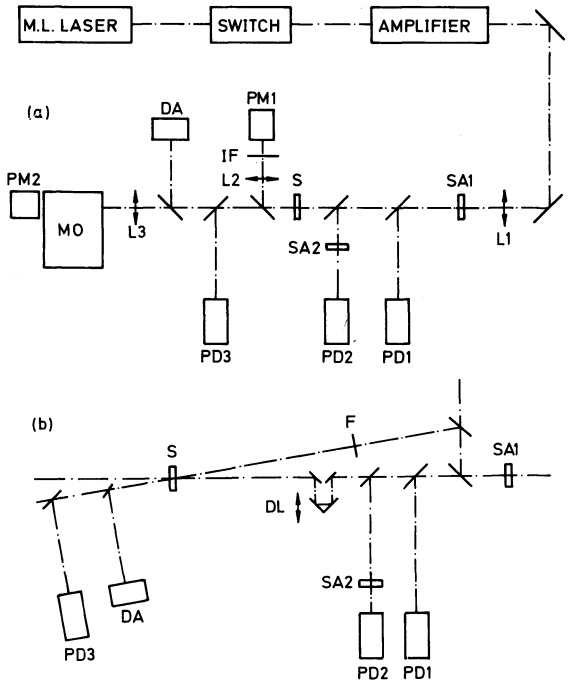

Figure 2 (a) Experimental arrangement for two-photon absorption and two-photon-induced emission measurements. (b) Pump and probe arrangement for absorption recovery measurement. L1 to L3, Lenses; SA1, SA2, saturable absorbers (Kodak dye No. 9860); PD1 to PD3, photodetectors; S, GaAs crystal; PM1, PM2, photomultipliers with S1 characteristic; IF, broad-band interference filter, MO, 25 cm grating monochromator; DA, linear silicon diode array; DL, optical delay line; F, filter.

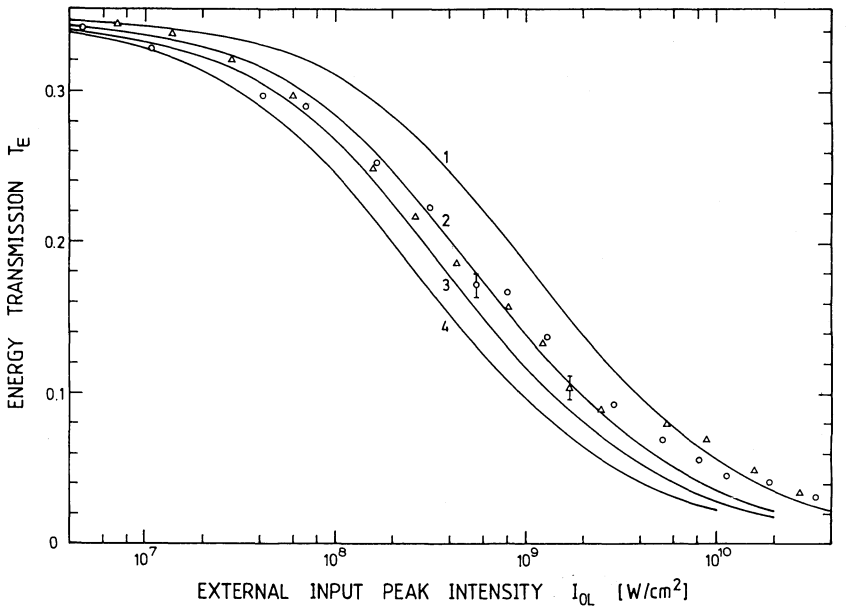

Figure 3 Energy transmission plotted against pump pulse peak intensity. 2.5 mm GaAs sample at (○) θ = 103 K and (△) θ = 295 K. The curves are calculated for $\alpha_1 = 1.57\,\mathrm{cm}^{-1}$ = constant (no EL2 level bleaching). 1, $\alpha^2 = 2 \times 10^{-8}\,\mathrm{cm\,W}^{-1}$; 2, $\alpha^{(2)} = 4 \times 10^{-8}\,\mathrm{cm\,W}^{-1}$; 3, $\alpha^{(2)} = 6 \times 10^{-8}\,\mathrm{cm\,W}^{-1}$; 4, $\alpha^{(2)} = 8 \times 10^{-8}\,\mathrm{cm\,W}^{-1}$.

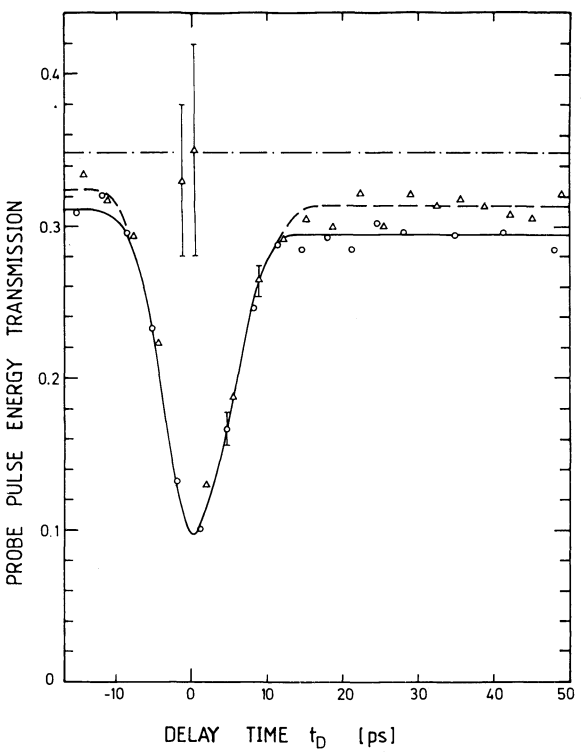

Figure 4 Probe pulse transmission plotted against delay time: 2.5 mm GaAs at (○—○) θ = 295 K and (△—△) θ = 103 K. (—·—) small signal transmission.

Energy transmission measurements were carried out at 295 and 103 K. The results are presented by the data points of Fig. 3.

The temporal behaviour of the non-linear absorption was studied in a pump and probe experiment. The experimental arrangement is shown in Fig. 2b. Two beamsplitters and a filter reduced the probe pulse intensity by a factor of 0.0025 compared with the pump pulse intensity.

The probe pulse transmission versus the delay time is shown in Fig. 4. The pump pulse peak intensity is adjusted to $3 \pm 1\,\mathrm{GW\,cm^{-2}}$. The temporal transmission profile follows the convolution of the probe and pump pulse. The probe pulse absorption is due to the simultaneous absorption of a probe pulse photon and a pump pulse photon ($\partial I_{\mathrm{pr}}(t)/\partial z = -\alpha^{(2)} I_{\mathrm{pr}}(t) I_{\mathrm{L}}(t + t_{\mathrm{D}})$; $\alpha^{(2)}$ is the two-photon absorption coefficient, I_{pr} is the probe pulse intensity, and I_{L} is the pump pulse intensity; t_{D} is the delay time). The trailing probe pulses do not completely reach the transmission of the leading probe pulses. This slight signal reduction is thought to be due to scattering losses. The diode array indicates probe beam distortions for the trailing probe pulses. A bleaching of the EL2 centre absorption with slow absorption recovery should have caused an increased transmission of trailing probe pulses beyond the small signal transmission. Since this bleaching is not observed it is thought that the refilling of excited EL2 centres occurs within the pump pulse duration (absorption recovery time $\lesssim \Delta t_{\mathrm{L}}$).

In the case of GaAs at 103 K a self-diffraction (two-wave mixing) of the pump pulse into the probe pulse direction was observed at optimum temporal overlap leading to high probe pulse transmissions (experimental points around $t_{\mathrm{D}} = 0$) [46, 47].

2.3. Spontaneous and stimulated emission

The two-photon-induced fluorescence of the GaAs crystal and the single-photon-induced fluorescence of the EL2 centres in the forward direction were investigated with the experimental arrangement of Fig. 2a. The emission in the forward direction was detected with photomultiplier PM1. The solid angle of observation was $\Delta\Omega_{\mathrm{A}} = 0.049\,\mathrm{sr}$ ($\Delta\Omega_{\mathrm{A}} = \pi d_{\mathrm{A}}^2/(4 l_{\mathrm{SL}}^2)$, d_{A} being the diameter of lens L2, and l_{SA} the distance between the GaAs sample and lens L2). The spectral distribution of the fluorescence signal was measured with the monochromator MO and the photomultiplier PM2. The angular distribution of the fluorescence signal was determined separately by moving the apertured photomultiplier PM1 around the sample S.

The normalized fluorescence signal $W_{\mathrm{F,out}}(\Delta\Omega_{\mathrm{A}})/W_{\mathrm{L,in}}$ is plotted against the input pump pulse intensity $I_{0\mathrm{L}}$ in Fig. 5. $I_{0\mathrm{L}}$ is the input peak intensity outside the sample. $W_{\mathrm{L,in}}$ is the input pump pulse energy outside the sample and $W_{\mathrm{F,out}}(\Delta\Omega_{\mathrm{A}})$ is the energy of the fluorescence signal behind the sample, which is directed to the photomultiplier. The solid curves belong to $\vartheta \simeq 103\,\mathrm{K}$ while the dashed curves are measured at $\vartheta \simeq 295\,K$. For curve 1 (circles and dots) the sample length is $l = 2.5\,\mathrm{mm}$ and the pump pulse diameter is approximately 0.5 mm (FWHM). At low intensities ($I_{0\mathrm{L}} < 2 \times 10^8\,W/\mathrm{cm}^2$) the fluorescence signal is dominated by population of the conduction band due to El2 centre absorption. The decrease of the fluorescence is caused by the enhanced conduction band to EL2 center recombination with decreasing EL2 level population (see computer simulations below, Fig. 19 and Fig. 20). At high intensities ($I_{0\mathrm{L}} > 5 \times 10^8\,W/\mathrm{cm}^2$) the two-photon induced fluorescence dominates. The curves 2 (open and filled triangles) and 3 (open and filled squares) belong to a sample length of $l = 0.5\,\mathrm{mm}$ and a pump pulse diameter of approximately 0.1 mm (FWHM). The signal of the curves 2 (triangles) is enhanced by longitudinal amplified spontaneous emission. The samples are strongly tilted to avoid laser oscillation

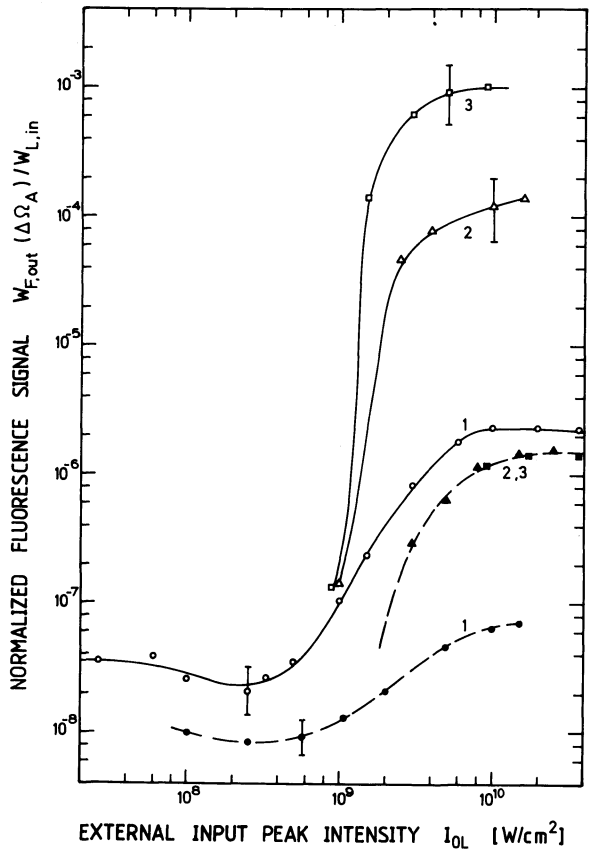

Figure 5 Fluorescence signal emitted in the forward direction. Solid angle of acceptance $\Delta\Omega_A$ = 0.049 sr. (——) θ = 103 K, (– – –) θ = 295 K. Curves 1 (●, ○), 2.5 mm GaAs (pump beam diameter (FWHM) ≈ 0.5 mm), signal is mainly due to spontaneous emission. Curves 2 (▲, △), 0.5 mm GaAs (pump beam diameter (FWHM) ≈ 0.1 mm), tilting angle ≈ 8°, signal is due to amplification of spontaneous emission. Curves 3 (■, □), 0.5 mm GaAs (pump beam diameter (FWHM) ≈ 0.1 mm) at normal incidence, signal at low temperature is enhanced by feedback (laser oscillation).

(tilting angle ≃ 8°, path of reflected light is not along the region excited by the pump pulse). The light is found to be unpolarized. For curve 3 (squares) the sample surfaces are normal to the input pump pulse. An enhanced signal due to laser oscillation is observed at low temperature ($\vartheta \simeq$ 103 K) while at room temperature no signal enhancement by feedback is observed. At high intensities the fluorescence signal of the 2.5 mm long samples is considerably less than the fluorescence signal of the 0.5 mm sample. This behaviour is thought to be due to reabsorption of the amplified spontaneous emission signal in the longer sample. A detailed analysis of the fluorescence curves is tried below by computer simulations.

The spectral distributions are presented in Fig. 6 ($I_{0L} \simeq 5 \times 10^9$ W/cm^2). The angular distribution of the amplified spontaneous emission (0.5 mm GaAs at 103 K, tilting angle 8°, solid curve 2 of Fig. 5, $I_{0L} \simeq 5 \times 10^9$ W/cm^2) is depicted in Fig. 7. The pedestal is due to spontaneous emission and amplified spontaneous emission into all directions. Practically the same result is obtained for the laser action in GaAs at low temperature (solid curve 3 of Fig. 5).

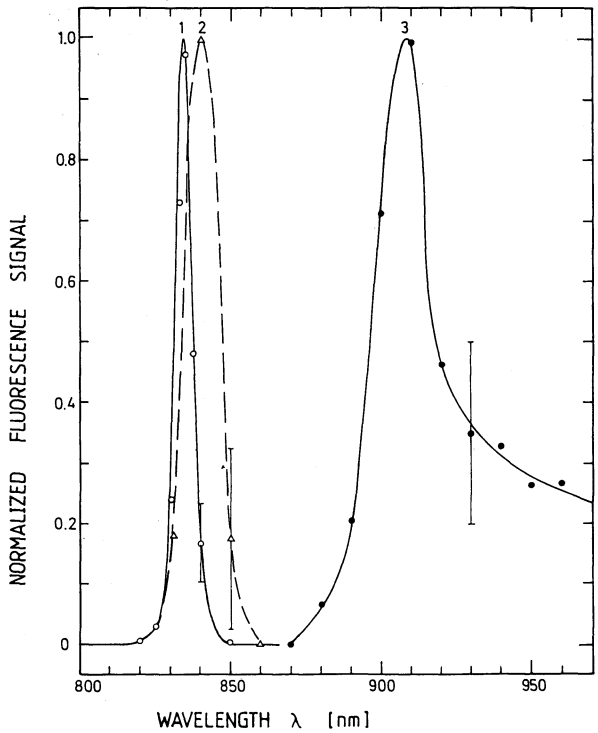

Figure 6 Spectral distribution of emission. Curve 1 (○), 0.5 mm GaAs normal to pump laser at θ = 103 K; curve 2 (△), 2.5 mm GaAs at θ = 103 K; curve 3 (●), 2.5 mm GaAs at θ = 295 K.

From the spontaneous emission data at low pump pulse intensities (Fig. 5, curve 1) the internal fluorescence quantum efficiency η_{int} may be determined approximately [48] by $\eta_{int} = W_{F,int}/W_{L,abs}$, with $W_{F,int} = W_{F,out}(\Delta\Omega_A)4\pi n_F^2/[\Delta\Omega_A(1 - R_F)]$ and $W_{L,abs} \approx (1 - R_L)W_{L,in} - W_{L,out}/(1 - R_L) = W_{L,in}[(1 - R_L) - T_E/(1 - R_L)]$. The result is

$$\eta_{int} \approx \frac{W_{F,out}(\Delta\Omega_A)}{W_{L,in}} \frac{4\pi n_F^2}{\Delta\Omega_A(1 - R_F)[(1 - R_L) - T_E/(1 - R_L)]} \tag{5}$$

where n_F and R_F are the refractive index and the reflectance, respectively, of GaAs at the fluorescence frequency. R_L is the reflectance at the pump laser frequency. The values of $W_{F,out}(\Delta\Omega_A)/W_{L,in}$ of 3.6×10^{-8} and 1.3×10^{-8} at $I_{OL} \approx 10^7$ W cm^{-2} for 103 and 295 K correspond to internal quantum efficiencies of $\eta_{int} \approx 8 \times 10^{-4}$ and 3×10^{-4}, respectively. The radiative lifetime, τ_{rad}, of GaAs with free-electron number density $N_{C,EQ} = 1.5 \times 10^{17}$ cm^{-3} is $\tau_{rad} \approx 7 \times 10^{-8}$ s [24] according to the van Roosbroeck–Shockley relation [49]. The estimated fluorescence lifetimes are $\tau_F = \tau_{rad}\eta_{int} \approx 55$ ps ($\theta \approx$ 103 K) and 20 ps ($\theta \approx$ 295 K). The short fluorescence lifetime of 20 ps explains why no effects of laser oscillation are observed at room temperature (dashed curve 3 of Fig. 5, round-trip time in 0.5 mm thick GaAs is 12 ps).

The fluorescence quantum efficiency of GaAs excited by interband single-photon absorption was measured with a spectrofluorometer applying the front-face collection technique [48]. The excitation wavelength was 527 nm and the sample temperature was 103 K. A

methanolic rhodamine 6G dye solution served as reference. The internal fluorescence quantum efficiency was determined to be $\eta_{int} \leqslant 8 \times 10^{-5}$. The resultant fluorescence lifetime is $\tau_F \leqslant 6$ ps. The excitation light was absorbed at the surface (penetration depth $l_{eff} = 1/\alpha \approx 0.1\,\mu$m [50]). A comparison of the single- and two-photon excitation data indicates that the surface fluorescence lifetime is at least a factor of 9 shorter than the bulk fluorescence lifetime.

3. Theory

The band structure of GaAs is shown in Fig. 8. The EL2 level is included [33]. Representative two-photon absorption transitions from the heavy-hole valence band (V1), the light-hole valence band (V2) and the split-off valence band (V3) to the conduction band (C) are indicated ($2\nu_L$). The single-photon absorption (transition from 1 to 2) excites the EL2 centres and contributes to the free carrier generation in the conduction band [35]. Absorption cross-sections of $\sigma_I = 1 \times 10^{-16}$ [36, 41] and 1.5×10^{-16} cm^2 [32] have been reported. The ionized EL2 centres may be refilled by single-photon absorption from the valence band (cross-section σ_V). The absorption cross-section values of $\sigma_V = 0.6\sigma_I$ (77 to 300 K) [33], $0.3\sigma_I$ [51], $0.23\sigma_I$ (300 K) [41], $0.11\sigma_I$ (78 K) [41] and $0.09\sigma_I$ [32] have been reported. The probe pulse transmission measurements of Fig. 4 indicate a rapid refilling of excited EL2 centres within the pump rate pulse duration ($\Delta t_L \approx 5$ ps), either by relaxation of excited centres or by filling of ionized centres from the conduction and valence bands. The photo-excited electrons in the conduction band recombine radiatively and non-radiatively with the photo-excited holes. n-type GaAs has a fluorescence band in the frequency region of the Nd : glass laser [52–55]. This fluorescence band may be due to deep centre impurities. Between these levels stimulated emission at the laser frequency may occur. Between the filled states of the conduction band and the empty states of the valence band spontaneous emission, amplified spontaneous emission and laser oscillation may occur (average frequency ν_F).

The following rate equation system describes the two-photon and single-photon absorption dynamics in GaAs with EL2 deep-level centres. The spontaneous emission is included. The amplified spontaneous emission is considered in an approximate manner (the spectral amplified spontaneous emission (ASE) signal distribution is not resolved; only an effective gain coefficient A_F is considered):

$$\begin{aligned}\frac{\partial N_C}{\partial t'} &= \frac{\alpha^{(2)}}{2h\nu_L} I_L^2 + k_{12C} N_{I2} - \frac{A_L}{h\nu_L}(N_C N_V - N_i^2) I_L - \frac{A_F}{h\nu_F}(N_C N_V - N_i^2) I_F \\ &\quad - k_{CV}(N_C N_V - N_i^2) - k_{CI}(N_C - N_{C,EQ})(N_I - N_{I1} - N_{I2}) \\ &\quad - k_{NR}(N_C - N_{C,EQ}) + \frac{\alpha_F}{h\nu_F} I_F \end{aligned} \tag{6}$$

$$\begin{aligned}\frac{\partial N_V}{\partial t'} &= \frac{\alpha^{(2)}}{2h\nu_L} I_L^2 + \frac{\sigma_V}{h\nu_L}(N_I - N_{I1} - N_{I2}) I_L - \frac{A_L}{h\nu_L}(N_C N_V - N_i^2) I_L \\ &\quad - \frac{A_F}{h\nu_F}(N_C N_V - N_i^2) I_F - k_{CV}(N_C N_V - N_i^2) - k_{IV}(N_V - N_{V,EQ}) N_{I1} \\ &\quad - k_{NR}(N_C - N_{C,EQ}) \frac{N_{I1} + N_{I2}}{N_I} + \frac{\alpha_F}{h\nu_F} I_F \end{aligned} \tag{7}$$

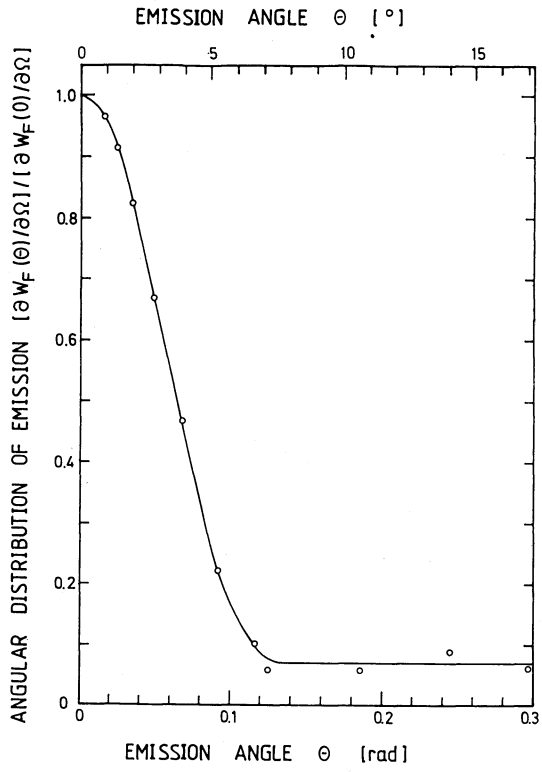

Figure 7 Angular distribution of emission. 0.5 mm GaAs at θ = 103 K. Tilting angle $\approx 8°$.

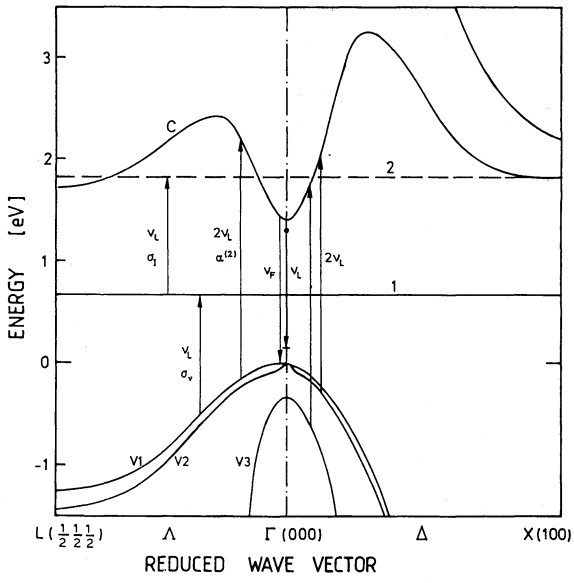

Figure 8 Band structure of GaAs (taken from [44]). Vertical scale applies to 300 K. V1, heavy hole; V2, light hole; V3, split-off valence band. C, conduction band. 1, Ground state level of EL2 centres; 2, excited state of EL2 centres. The transitions are indicated.

$$\frac{\partial N_{I1}}{\partial t'} = -\frac{\sigma_I}{h\nu_L} N_{I1} I_L + \frac{\sigma_V}{h\nu_L}(N_I - N_{I1} - N_{I2}) I_L + k_I N_{I2}$$
$$+ k_{CI}(N_C - N_{C,EQ})(N_I - N_{I1} - N_{I2}) - k_{IV}(N_V - N_{V,EQ}) N_{I1}$$
$$+ k_{NR}(N_C - N_{C,EQ}) \frac{N_I - N_{I1} - N_{I2}}{N_I} \tag{8}$$

$$\frac{\partial N_{I2}}{\partial t'} = \frac{\sigma_I}{h\nu_L} N_{I1} I_L - k_{I2C} N_{I2} - k_I N_{I2} \tag{9}$$

$$\frac{\partial I_{L,F1}(t')}{\partial z} = -\alpha^{(2)} I_L I_{L,F1} - \sigma_I N_{I1} I_{L,F1} - \sigma_V (N_I - N_{I1} - N_{I2}) I_{L,F1}$$
$$+ A_L (N_C N_V - N_i^2) I_{L,F1} - \sigma_{FC} N_C I_{L,F1} - \sigma_{FV} N_V I_{L,F1} \tag{10}$$

$$\frac{\partial I_{L,B1}[t' - 2(l-z)n/c_0]}{\partial z} = -\alpha^{(2)} I_L I_{L,B1} - \sigma_I N_{I1} I_{L,B1} - \sigma_V (N_I - N_{I1} - N_{I2}) I_{L,B1}$$
$$+ A_L (N_C N_V - N_i^2) I_{L,B1} - \sigma_{FC} N_C I_{L,B1} - \sigma_{FV} N_V I_{L,B1} \tag{11}$$

$$\frac{\partial I_{L,F2}(t' - 2nl/c_0)}{\partial z} = -\alpha^{(2)} I_L I_{L,F2} - \sigma_I N_{I1} I_{L,F2} - \sigma_V (N_I - N_{I1} - N_{I2}) I_{L,F2}$$
$$+ A_L (N_C N_V - N_i^2) I_{L,F2} - \sigma_{FC} N_C I_{L,F2} - \sigma_{FV} N_V I_{L,F2} \tag{12}$$

$$\frac{\partial I_F}{\partial z} = h\nu_F \frac{\Delta\Omega_A}{4\pi} k_{CV}(N_C N_V - N_i^2) + A_F (N_C N_V - N_i^2) I_F - \alpha_F I_F \tag{13}$$

The transformation $t' = t - nz/c_0$ is used (n is the refractive index and c_0 the speed of light *in vacuo*). I_L is an abbreviation for $I_{L,F1}(t', z) + I_{L,B1}[t' - 2(l-z)n/c_0, z] + I_{L,F2}(t' - 2nl/c_0, z)$. The initial level populations are $N_C(t' = -\infty, z) = N_{C,EQ}$, $N_V(-\infty, z) = N_{V,EQ}$, ($N_{C,EQ} N_{V,EQ} = N_i^2$, N_i being the intrinsic carrier concentration at temperature θ), $N_{I1}(-\infty, z) = N_I$ (number density of EL2 centres) and $N_{I2}(-\infty, z) = 0$.

The initial condition of the input light is $I_{L,F1}(t', r, z = 0) = I_{L,in}(t', r)(1 - R_L)$, with $I_{L,in}(t', r) = I_{0L} \exp(-r^2/r_0^2) \exp(-t'^2/t_0^2)$. r_0 is the $1/e$ beam radius and t_0 is half the $1/e$ pulse duration ($t_0 = \Delta t_L/[2(\ln 2)^{1/2}]$). The boundary condition of the light reflected back at the exit surface of the crystal is $I_{L,B1}(t', r, z = l) = R_L I_{L,F1}(t', r, z = l)$. Part of $I_{L,B1}$ is reflected in the forward direction according to $I_{L,F2}(t' - 2nl/c_0, r, z = 0) = R_L I_{L,B1}(t' - 2nl/c_0, r, z = 0)$. The two-photon absorption of further light reflected back-and-forth is neglected, and only the linear loss is included in the time-integrated transmission formula, which is

$$T_{TI} = \frac{w_{L,out}(r)}{w_{L,in}(r)} = \frac{\int_{-\infty}^{\infty} I_{L,out}(t', r)\, dt'}{\int_{-\infty}^{\infty} I_{L,in}(t', r)\, dt'} \tag{14}$$

with

$$I_{L,out}(t', r) = (1 - R_L)$$
$$\times \left[I_{L,F1}(t', r, l) + I_{L,F2}(t' - 2nl/c_0, r, l) \left(1 + R_L^2 \frac{\exp(-2\sigma_I N_I l)}{1 - R_L^2 \exp(-2\sigma_I N_I l)} \right) \right] \tag{15}$$

The energy transmission is

$$T_E = \frac{\int_0^\infty w_{out}(r)\,dr}{\int_0^\infty w_{in}(r)\,dr} \tag{16}$$

The initial condition of the fluorescence signal is $I_F(t' = -\infty, r, z) = 0$.

The calculations indicate that the two-photon absorption of the light, $I_{L,B1}$, reflected back is negligible and has no measurable influence on the two-photon absorption and emission dynamics. Therefore, Equations 11 and 12 are dropped and $I_L(t', r, z)$ is set equal to $I_{L,F1}(t', r, z)$. Equation 15 reduces to

$$I_{L,out}(t', r) = (1 - R_L)I_L(t', r, l)\left(1 + R_L^2 \frac{\exp(-2\sigma_1 N_I l)}{1 - R_L^2 \exp(-2\sigma_1 N_I l)}\right) \tag{17}$$

Equation 6 describes the population dynamics of the conduction band. The first term is due to two-photon absorption. The second term fills the conduction band from the excited impurity level. k_{I2C} is the relevant unimolecular rate constant. The third and fourth terms take care of the stimulated emission at the pump laser frequency ν_L and the fluorescence frequency ν_F, respectively. The factors $A_L N_V$ and $A_F N_V$ resemble the stimulated emission cross-sections. The next two terms give the radiative relaxations to the valence band and to the deep-level impurity centres. k_{CV} and k_{CI} are the relevant bimolecular rate constants [56]. The penultimate term considers non-radiative relaxation. Auger recombination is not included. This process is thought to be negligible for the free carrier concentrations achieved experimentally [57]. The last term gives the population of the conduction band by fluorescence light reabsorption.

The population dynamics of the free carriers in the valence band is handled by Equation 7. The first term gives the hole production by two-photon absorption. The second term is due to transitions from the valence band to ionized impurity centres. The third and fourth terms give the stimulated emission at the pump laser frequency and the fluorescence frequency, respectively. The fifth term takes care of radiative electron–hole recombination from the conduction band to the valence band. The sixth term gives the hole-filling by impurity ionization. The seventh term reduces the hole concentration by non-radiative relaxations, and the last term gives the hole generation by fluorescence reabsorption.

Equations 8 and 9 describe the deep-level centre (EL2) dynamics. The terms of Equation 8 give the single-photon excitation (first), the absorptive level filling from the valence band (second), the intra-impurity relaxation [35, 40] (third), the relaxation from the conduction band (fourth) and from the valence band (fifth). The last term considers the non-radiative relaxation from the conduction band to the impurity levels. The terms of Equation 9 are due to single-photon excitation, impurity-to-conduction band relaxation and intra-impurity relaxation.

The pump pulse propagation is given by Equations 10 to 12. The input pulse $I_{L,F1}$, the first back-reflected pulse $I_{L,B1}$ and the next forward-reflected contribution $I_{L,F2}$ are handled. The first terms are due to two-photon absorption, the second terms give the single-photon absorption of the impurities, the third terms give the single-photon transitions from the valence band to ionized impurities, the fourth terms take care of the stimulated emission of the laser light, and the last two terms are due to free-electron and free-hole absorption.

The fluorescence signal is described by Equation 13. The first term gives the radiative recombination of electrons and holes (spontaneous emission). $\Delta\Omega_A$ is the solid angle of

observation. The second term describes the stimulated emission (amplified spontaneous emission). The last term takes care of the fluorescence reabsorption in an approximate manner. α_F is an average absorption coefficient in the fluorescence region.

4. Computer simulations

The two-photon absorption and emission dynamics of GaAs is analysed in the following. The parameters of Table I are applied (temperature $\theta = 103\,K$, sample length $l = 2.5\,mm$) except where stated otherwise.

4.1. Influence of two-photon absorption coefficient

The curves in the Figs 3 and 9 to 11 are calculated without involving the absorption dynamics of the EL2 centres; that is, $N_{I1} = N_I$, $N_{I2} = 0$, $\alpha_I = N_I\sigma_I = 1.57\,cm^{-1}$. It is assumed that the linear absorption does not generate free carriers. In addition, the stimulated emission at the pump laser frequency ν_L and at the fluorescence frequency ν_F are neglected; that is, $A_L = A_F = 0$.

The calculated energy transmission curves are presented in Fig. 3. The two-photon absorption equations (Equations 10 to 12) reduce to $\partial I_L/\partial z = -\alpha^{(2)}I_L^2 - \alpha_I I_L - (N_C\sigma_{FC} + N_V\sigma_{FV})I_L$. The first two terms have been applied in previous two-photon absorption analyses of GaAs [1–16]. The transmission loss by free-carrier absorption is negligible. For input peak intensities of $I_{0L} \lesssim 3 \times 10^9\,W\,cm^{-2}$ the experimental points follow the theoretical dependences reasonably well. Above $3 \times 10^9\,W\,cm^{-2}$ the experimental transmissions are higher than expected from the theory.

The length-integrated photogenerated free-electron number density at $t' = \Delta t_L$ and $r = 0$, $\int_0^l N_C(t' = \Delta t_L, r = 0, z)\,dz - N_{C,EQ}l$, is shown in Fig. 9 for three different two-photon absorption coefficients. At low intensities the excess free-electron number density rises quadratically with the pump pulse intensity. At high pump intensities the rise of the

TABLE I Parameters of the GaAs sample

Parameter	$\theta = 103\,K$		$\theta = 295\,K$	References
$\alpha^{(2)}$ ($cm\,W^{-1}$)	$(4.5 \pm 1) \times 10^{-8}$		$(4.5 \pm 1) \times 10^{-8}$	This work
σ_I (cm^2)	1×10^{-16}		1×10^{-16}	36
σ_V (cm^2)	6×10^{-17}		6×10^{-17}	33
σ_{FC} (cm^2)		9×10^{-20}		*
σ_{FV} (cm^2)		9×10^{-20}		Assumed
α_F (cm^{-1})		2		Assumed
A_L (cm^5)	$(2 \pm 1) \times 10^{-35}$		$(2 \pm 1) \times 10^{-35}$	This work
A_F (cm^5)	$\sim 10^{-33}$		$\sim 3 \times 10^{-34}$	This work
k_{CV} ($cm^3\,s^{-1}$)		10^{-10}		24
k_{I2C} ($cm^3\,s^{-1}$)		∞		Assumed
k_I (s^{-1})		10^9		Assumed
k_{CI} ($cm^3\,s^{-1}$)		$> 10^{-5}$		This work†
k_{IV} ($cm^3\,s^{-1}$)		10^{-10}		Assumed
k_{NR} (s^{-1})	1.8×10^{10}		5×10^{10}	This work
N_i (cm^{-3})	3×10^{-18}		1.4×10^6	44
$N_{C,EQ}$ (cm^{-3})		1.5×10^{17}		This crystal

* Extrapolated from [65].

† Value is estimated from missing transmission over-shoot in Fig. 4; $k_{CI} = 10^{-4}\,cm^3\,s^{-1}$ is used in calculations.

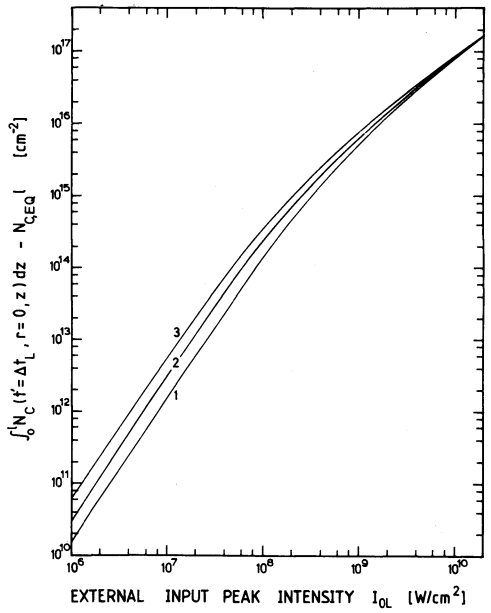

Figure 9 Length-integrated excess conduction band population, $\int_0^{l'} N_C(t' = \Delta t_L, r = 0, z)\,dz - N_{C,EQ}l$, plotted against input pump pulse peak intensity. EL2 centres are not bleached and do not populate the conduction band. Stimulated emission at ν_L and ν_F is not included; that is, $A_L = A_F = 0$. Otherwise parameters of Table I apply (θ = 103 K, l = 2.5 mm). Curve 1, $\alpha^{(2)} = 2 \times 10^{-8}$ cm W^{-1}; curve 2, $\alpha^{(2)} = 4 \times 10^{-8}$ cm W^{-1}; curve 3, $\alpha^{(2)} = 8 \times 10^{-8}$ cm W^{-1}.

free-electron number density changes to a linear dependence (the free-electron concentration is proportional to the absorbed light, and at high pump intensities practically all light is absorbed).

The excess free-electron concentration, $N_C(t' = \Delta t_L, r = 0, z) - N_{C,EQ}$, is plotted against the sample length in Fig. 10 for various input pulse intensities. At low intensities the excess free-carrier concentration decreases slightly with distance, because of light reduction by linear absorption. At high pump pulse intensities the excess carrier concentration becomes very high at the entrance region, because of strong pump pulse reduction by two-photon absorption. The inclusion of the two-photon absorption of the back-reflected pulse leads to a slight wrapping-up of the excess free-carrier concentration at the exit surface.

The spontaneous emission behaviour is illustrated in Fig. 11. The solid curves show the normalized spontaneous emission signals $w_{F,out}(\Delta\Omega_A)/w_{L,in} = \int_{-\infty}^{\infty} I_{F,out}(t', r = 0, \Delta\Omega_A)\,dt' / \int_{-\infty}^{\infty} I_{L,in}(t', r = 0)\,dt'$ for three different two-photon absorption coefficients. The broken curves give the internal fluorescence quantum efficiency $\eta_{int} = w_{F,int}/w_{L,abs}$ (compare Equation 5). The curves are calculated for a recombination rate constant of $k_{CV} = 10^{-10}$ cm^3 s^{-1} and a non-radiative rate constant of $k_{NR} = 1.8 \times 10^{10}$ s^{-1} (Table I). Below $I_{0L} = 2 \times 10^8\, W/\text{cm}^2\,\tau_{rad}$ is approximately constant (determined by $N_{C,EQ}$) and the fluorescence signal rises with the two-photon absorption. Above $I_{0L} = 5 \times 10^8\, W/\text{cm}^2\,\tau_{rad}$ becomes shortened ($N_C > N_{C,EQ}$) and the fluorescence signal rises steeply. The radiative rate $k_{CV}N_V$ dominates over the nonradiative rate k_{NR} and the internal fluorescence quantum efficiency approaches unity.

4.2. Influence of stimulated emission at ν_L

The occurrence of fluorescence light at $\lambda_L = 1.06\,\mu$m [52–55] indicates the presence of stimulated emission at the laser frequency ν_L. The influence of stimulated emission at ν_L is investigated in the following. The absorption dynamics of the EL2 centres is still neglected,

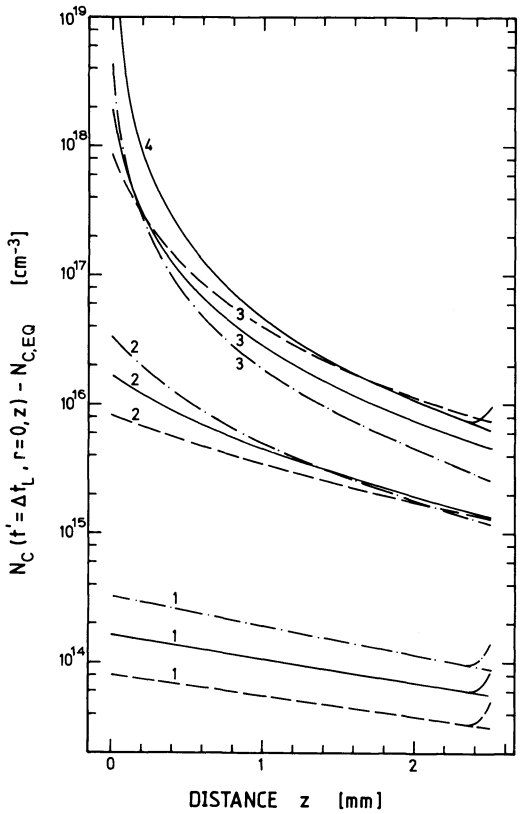

Figure 10 Excess free-electron number density of conduction band, $N_C(t' = \Delta t_L, r = 0, z) - N_{C,EQ}$, plotted against sample length. Parameters of Fig. 9 apply. (——) $\alpha^{(2)} = 4 \times 10^{-8}$ cm W^{-1}, (— —) $\alpha^{(2)} = 2 \times 10^{-8}$ cm W^{-1}, (—·—) $\alpha^{(2)} = 8 \times 10^{-8}$ cm W^{-1}. Curves 1, $I_{0L} = 3 \times 10^{7}$ W cm^{-2}; curves 2, $I_{0L} = 3 \times 10^{8}$ W cm^{-2}; curves 3, $I_{0L} = 3 \times 10^{9}$ W cm^{-2}; curve 4, $I_{0L} = 2 \times 10^{10}$ W cm^{-2}. The wrap-up of curves 1 and 4 at the end of the sample is obtained if the back-reflection of the pump pulse is included in the analysis (Equations 10 to 12).

as in Section 4.1. It is again assumed that the linear absorption does not generate free carriers. The amplification of spontaneous emission is not included; that is, $A_F = 0$.

The influence of the stimulated emission at the pump laser frequency ν_L on the energy transmission is investigated in Fig. 12. The stimulated emission coefficient A_L is varied. The two-photon absorption coefficient is set to $\alpha^{(2)} = 4.5 \times 10^{-8}$ cm W^{-1}. The stimulated emission increases the transmission at high pump pulse intensities (higher N_C-values). With increasing A_L-values the rise of transmission shifts to lower intensities. At high intensities the measured energy transmissions remain above the calculated curves. Slight deviations of the pump pulses from Gaussian shape and pump pulse distortion inside the sample are thought to be responsible for the increased energy transmission. The influence of the stimulated emission at the pump laser frequency on the two-photon absorption dynamics of organic dyes was studied in detail in [58, 59].

The length-integrated photogenerated free-electron number density at $t' = \Delta t_L$ and $r = 0$, $\int_0^l N_C(t' = \Delta t_L, r = 0, z)\, dz - N_{C,EQ} l$, is plotted in Fig. 13 for various A_L-values. The stimulated emission reduces the free-carrier generation at high pump pulse intensities. The influence of the n-type doping is illustrated. High doping reduces the excess carrier density because of enhanced recombination.

The excess free-carrier distribution, $N_C(t' = \Delta t_L, r = 0, z) - N_{C,EQ}$, is plotted against the sample length in Fig. 14 for some pump pulse intensities and stimulated emission values. The lowering of the free-carrier concentration at the entrance region with increasing A_L-values is seen clearly.

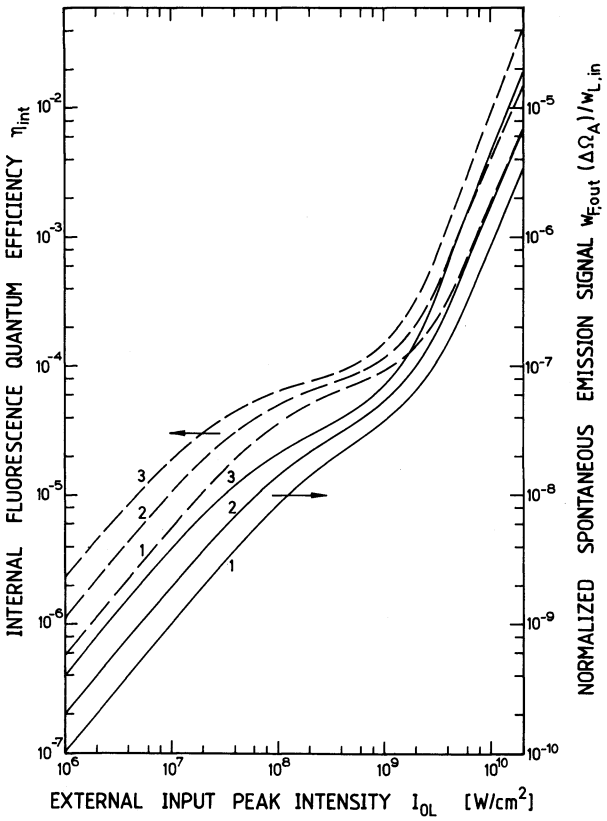

Figure 11 Spontaneous emission signal (——) and internal fluorescence quantum efficienty (— —). For legend see Fig. 9.

The normalized spontaneous emission, $w_{F,out}(\Delta\Omega_A)/w_{L,in}$, is plotted against the pump pulse input peak intensity in Fig. 15. The stimulated emission at the pump laser frequency reduces the fluorescence signal because of depopulation of the conduction band. The spontaneous emission increases with doping ($\partial I_F/\partial z \propto k_{CV}(N_C N_V - N_i^2) \approx k_{CV}(N_{C,EQ} + N_{C,excess})N_{C,excess}$).

4.3. Inclusion of EL2 absorption dynamics

The influence of the EL2 absorption dynamics on the two-photon transmission is analysed in Fig. 16. The two-photon absorption coefficient is set to $\alpha^{(2)} = 4.5 \times 10^{-8}\,\mathrm{cm\,W^{-1}}$. Stimulated emission is not included ($A_L = A_F = 0$). The small-signal absorption coefficient of the impurity centres is $\alpha_I = \sigma_I N_I = 1.57\,\mathrm{cm^{-1}}$. The EL2 excitation populates the conduction band ($k_{I2C} = \infty$). The bimolecular relaxation rate constant for the transition from the conduction band to the EL2 centres is set to $k_{CI} = 10^{-4}\,\mathrm{cm^3\,s^{-1}}$. For our experimental situation of $\sigma_I \approx 10^{-16}\,\mathrm{cm^2}$ [36, 41], $\sigma_V \approx (0.6 - 0.1)\sigma_I$ [32, 33, 41, 51] and $\alpha^{(2)} = 4.5 \times 10^{-8}\,\mathrm{cm\,W^{-1}}$ the EL2 absorption dynamics does not influence the two-photon transmission measurably.

The length-integrated excess free-electron number density and the length-integrated ground-state impurity centre number density are plotted in Fig. 17 for $A_L = A_F = 0$. The

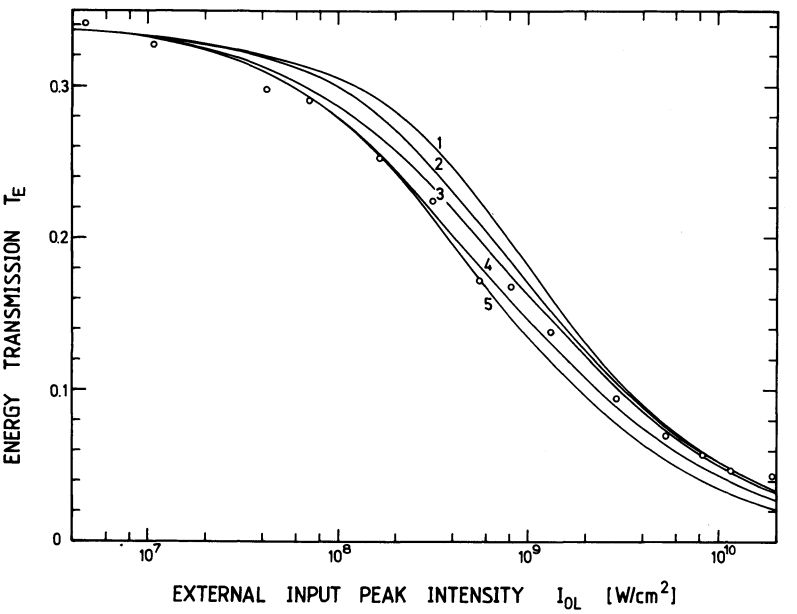

Figure 12 Influence of stimulated emission at ν_L on energy transmission. EL2 centres are not bleached and do not populate the conduction band ($\alpha_1 = N_1\sigma_1$ = constant). Amplification of spontaneous emission is not included; that is, $A_F = 0$. Otherwise parameters of Table I apply (θ = 103 K, l = 2.5 mm). $\alpha^{(2)} = 4.5 \times 10^{-8}$ cm W^{-1}. Curve 1, $A_L = 8 \times 10^{-32}$ cm^5 (same curve for $A_L = 2 \times 10^{-32}$ cm^5); curve 2, $A_L = 1 \times 10^{-32}$ cm^5; curve 3, $A_L = 5 \times 10^{-33}$ cm^5; curve 4, $A_L = 1 \times 10^{-33}$; curve 5, $A_L = 0$.

broken curves correspond to $k_{I2C} = 0$; that is, the EL2 centres are excited but do not populate the conduction band. The solid curves are calculated for $k_{I2C} = \infty$; that is, the excited EL2 centres transfer the excited electron immediately to the conduction band. The fast refilling from the conduction band hinders a bleaching of the EL2 centres (curves 1). All curves are independent of the doping concentration $N_{C,EQ}$ (since $A_L = A_F = 0$ is assumed).

The excess free-electron concentration, $N_C(t' = \Delta t_L, r = 0, z) - N_{C,EQ}$, is plotted against the sample length in Fig. 18 for $k_{I2C} = \infty$ and $k_{CI} = 10^{-4}$ cm^3 s^{-1} (see Table I). The solid curves are for $A_L = A_F = 0$ (no stimulated emission involved). The broken curve is calculated for $k_{I2C} = \infty$, $k_{CI} = 10^{-4}$ cm^3 s^{-1}, $A_L = 2 \times 10^{-35}$ cm^5 and $A_F = 0$. The chain-broken curve is obtained for $A_L = 3 \times 10^{-35}$ cm^5 and $A_F = 10^{-33}$ cm^5 (best-fit experimental parameters, see below). Compared with Figs 10 and 14 (EL2 centres are not involved in population of the conduction band) the photo-excited free-carrier concentration is increased by the ionization of the deep-level centres, especially at low pump pulse intensities (curves 1 and 2).

The intensity dependence of the spontaneous emission is analysed in Fig. 19. Amplified spontaneous emission is excluded by setting $A_F = 0$. The solid curves 1 and 1′ differ in k_{CI} (curve 1, $k_{CI} = 10^{-4}$ cm^3 s^{-1}; curve 1′, $k_{CI} = 0$). Large k_{CI}-values give a short absorption recovery time for the EL2 centres as observed experimentally (see Fig. 4). The spontaneous emission increases with doping (increase of $N_{C,EQ}$). The stimulated emission at the laser frequency ν_L quenches the spontaneous emission. The solid and short-broken curves of Fig. 19 have to be compared with the solid and broken curve 1 of Fig. 5. (If the curve of

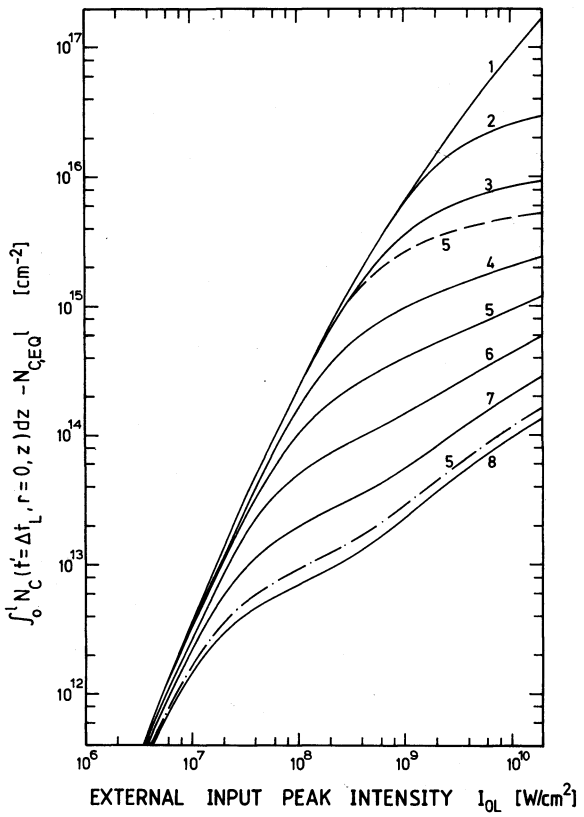

Figure 13 Influence of stimulated emission at ν_L on length-integrated excess free-electron number density of conduction band. For legend see Fig. 12. (——) $N_{C,EQ}$ = 1.5×10^{17} cm^{-3}, (— —) $N_{C,EQ} = 10^{16}$ cm^{-3}, (—·—) $N_{C,EQ} = 10^{18}$ cm^{-3}. The A_L-values of the curves are 1, 0; 2, 10^{-34} cm^5; 3, 10^{-33} cm^5; 4, 5×10^{-33} cm^5; 5, 10^{-32} cm^5; 6, 2×10^{-32} cm^5; 7, 4×10^{-32} cm^5; 8, 8×10^{-32} cm^5.

Fig. 19 are integrated over the spatial beam profile, they shift approximately a factor of two to the right). At low pump intensities the fit determines the non-radiative rate k_{NR} (see Table 1). At high pump intensities an accurate determination of A_L is not possible since the amplification of spontaneous emission ($A_F > 0$, Fig. 20) contributes to the experimental signal. For the 2.5 mm long sample at 295 K (broken curve 1 of Fig. 5) the ASE contribution is thought to be less important (smaller A_F-value at 295 K, and reabsorption of ASE-signal). The experimental curve can be fitted by the broken curve 2 of Fig. 19 ($A_L = 1 \times 10^{-35}$ cm^5). Considering ASE contributions a reasonable value is $A_L = (2 \pm 1) \times 10^{-35}$ cm^5. For the 2.5 mm long sample at 103 K (solid curve 1 of Fig. 5) the amplified spontaneous emission contributes stronger to the signal. A value of $A_L = (2 \pm 1) \times 10^{-35}$ cm^5 is compatible to the experimental curve.

The light generation by amplification of spontaneous emission is analysed in Fig. 20. The amplification of spontaneous emission becomes dominant as soon as the gain factor $A_F(N_C N_V - N_i^2) l_{TPA}$ becomes larger than one [60]. (l_{TPA} is the penetration depth of the pump laser which is limited by the two-photon absorption). Solid curve 1 is calculated for $A_L = 0$ and $A_F = 10^{-33}$ cm^5. Reflection losses limit the maximum conversion efficiency to $w_{F,out}/w_{L,in} \simeq (1 - R_F)(1 - R_L) \simeq 0.5$. The limitation of amplified spontaneous emission by free carrier absorption is negligible (σ_{FC} and σ_{FV} are too small). For the amplified spontaneous emission of single-photon [60] and two-photon [61] pumped organic dye solutions the excited-state absorption was an important parameter in the limitation of the conversion efficiency.

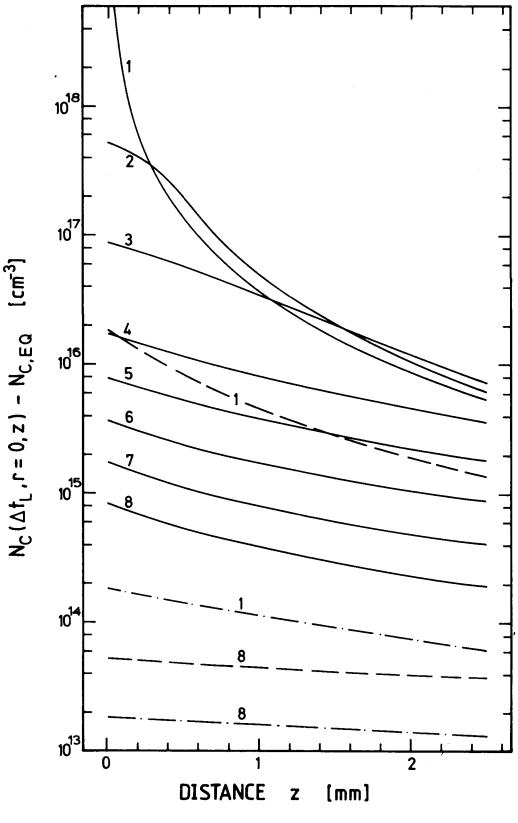

Figure 14 Influence of A_L on distribution of excess free-electron number density of conduction band. The legend of Fig. 12 applies. $N_{C,EQ} = 1.5 \times 10^{17}$ cm^{-3}. (——) $I_{0L} = 10^{10}$ W cm^{-2}, (— —) $I_{0L} = 3 \times 10^{8}$ W cm^{-2}, (—·—) $I_{0L} = 3 \times 10^{7}$ W cm^{-2}. The curves are for $A_L = 0$ (1), 10^{-34} cm^5 (2), 10^{-33} cm^5 (3), 5×10^{-33} cm^5 (4), 10^{-32} cm^5 (5), 2×10^{-32} cm^5 (6), 4×10^{-32} cm^5 (7) and 8×10^{32} cm^5 (8).

The curves of Fig. 20 have to be compared with experimental curve 2 of Fig. 5. The rise of solid curve 2 of Fig. 5 ($l = 0.5$ mm, $\vartheta = 103$ K) may be fitted by solid curve 2 of Fig. 20, but at high intensities this theoretical curve leads to higher conversion efficiencies than observed experimentally. It is thought that the small conversion efficiency of light emission in forward direction is caused by a change-over of the amplified spontaneous emission in forward direction to all angular directions or preferentially to transverse directions. The excess free carrier distribution of Fig. 18 indicates the accumulation of free carrier population at the entrance face of the crystal. The pump laser penetration depth becomes comparable to or shorter than the pump pulse beam diameter which favours the amplification of spontaneous emission in all spatial directions (penetration depth equal to beam diameter) or in transverse direction (penetration depth less than beam diameter) [62–64]. Even in the case of amplified spontaneous emission in all directions, an angular fluorescence signal distribution like that of Fig. 7 would be observed because the ASE signal outside the pump pulse direction would be reabsorbed in GaAs. An ASE signal emission into all directions would limit the maximum possible ASE-signal captured by the photomultiplier PM1 (Fig. 2a, $\Delta\Omega_A = 0.049$sr) to $w_{ASE,out}(\Delta\Omega_A)/w_{L,in} \simeq (1 - R_F)(1 - R_L)\Delta\Omega_A/(4\pi n_F^2) \simeq 1.5 \times 10^{-4}$. This value is obtained experimentally.

Solid curve 1 of Fig. 5 ($l = 2.5$ mm, $\vartheta = 103$ K) saturates at a lower conversion efficiency of approximately 2×10^{-6}. In this case the transverse amplified spontaneous emission is

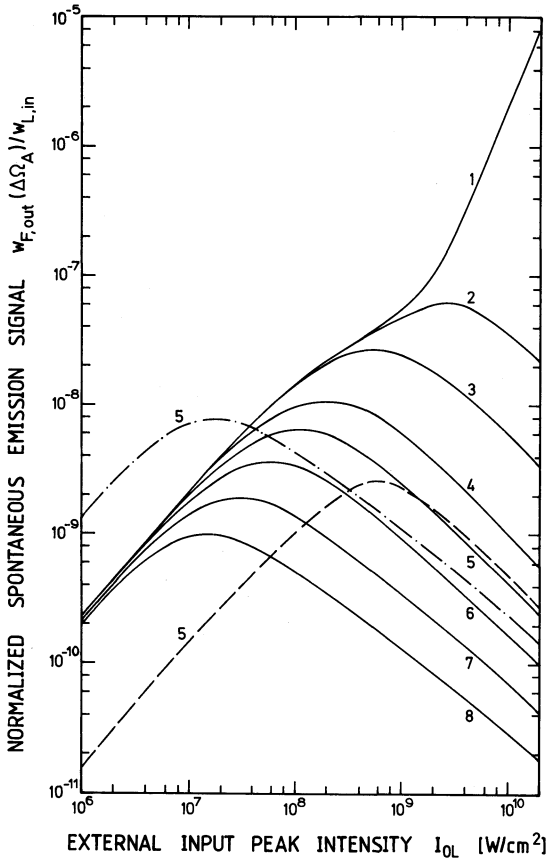

Figure 15 Influence of A_L on spontaneous emission. For legend see Figs 12 and 13.

dominant (larger pump beam diameter of about 0.5 mm) and the ASE signal in forward direction is reabsorbed (see Fig. 1a and Fig. 6).

For the 0.5 mm sample of GaAs at $\vartheta = 295$ K (broken curve 2 of Fig. 5) the onset of efficient amplified spontaneous emission occurs at higher intensities and the conversion efficiency saturates already at about 1.5×10^{-6}. This behaviour indicates a smaller effective emission coefficient A_F. Resonable values of A_F and A_L are $A_F \simeq 3 \times 10^{-34}\,\mathrm{cm}^5$ and $A_L \simeq (2 \pm 1) \times 10^{-35}\,\mathrm{cm}^5$.

The calculated temporal pulse shapes of the fluorescence and ASE signals are presented in Fig. 21 ($A_L = 3 = 10^{-35}\,\mathrm{cm}^5$, $A_F = 10^{-33}\,\mathrm{cm}^5$). The curves belong to various input pump intensities. The dotted curve gives the input pump pulse shape. Curve 4 represents the spontaneous emission at low pump pulse intensity ($I_{0L} = 10^6\,W/\mathrm{cm}^2$). Broken curve 3 ($I_{0L} = 10^8\,W/\mathrm{cm}^2$) indicates the enhanced depopulation of the conduction band by relaxation to the excited EL2 centres ($k_{CI} = 10^{-4}\,\mathrm{cm}^3\,\mathrm{s}^{-1}$). At high pump pulse intensities the amplification of spontaneous emission shortens considerably the signals. At $I_{0L} = 3 \times 10^9\,W/\mathrm{cm}^2$ the ASE pulse duration is 3 ps (curve 1).

5. Conclusions

The two-photon absorption dynamics and the two-photon-induced emission dynamics of n-type GaAs were studied experimentally and theoretically. The bleaching of the

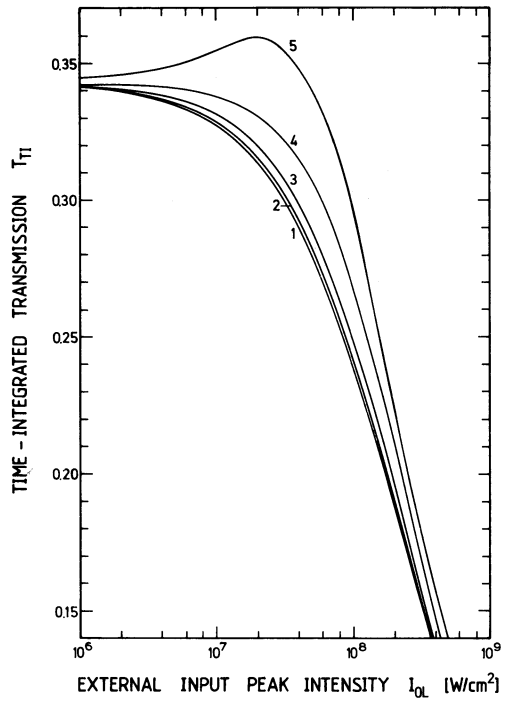

Figure 16 Influence of EL2 absorption dynamics on time-integrated transmission through the GaAs sample (l = 2.5 mm, θ = 103 K). A_L = A_F = 0. $\alpha_I = N_I\sigma_I$ is kept constant. Parameters are listed in Table I except (1) $\sigma_V = \sigma_I$ (independent of actual value of σ_I); (2) $\sigma_I = 10^{-16}$ cm^2 and $\sigma_V = 0$; (3) $\sigma_I = 10^{-15}$ cm^2 and $\sigma_V = 0.6\sigma_I$; (4) $\sigma_I = 10^{-15}$ cm^2 and $\sigma_V = 0$; (5) $\sigma_I = 3 \times 10^{-15}$ cm^2 and $\sigma_V = 0$.

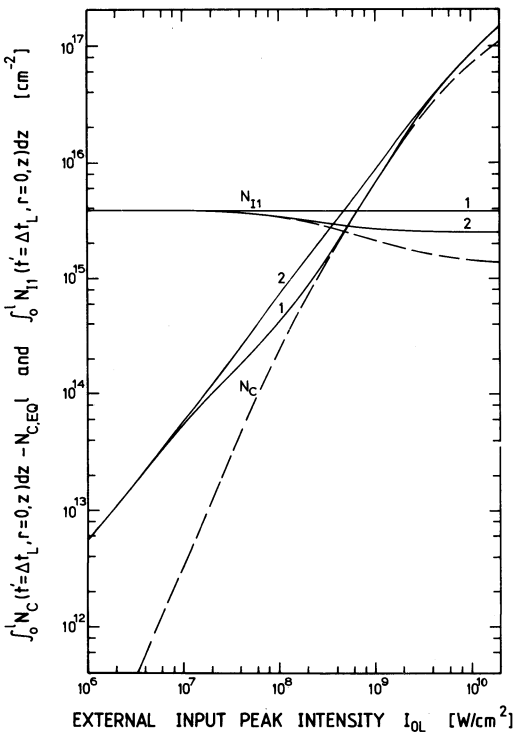

Figure 17 Influence of EL2 absorption dynamics on length-integrated excess free-electron number density of conduction band, N_C, and on length-integrated ground-state EL2 centre number density, N_{I1}. For legend see Fig. 16. $\sigma_I = 10^{-16}$ cm^2, $\sigma_V = 0.6\sigma_I$. (— —) $k_{I2C} = 0$ (EL2 excitation does not contribute to free carrier generation); (——) $k_{I2C} = \infty$ with (1) $k_{CI} = 10^{-4}$ cm^3 s^{-1} and (2) $k_{CI} = 0$.

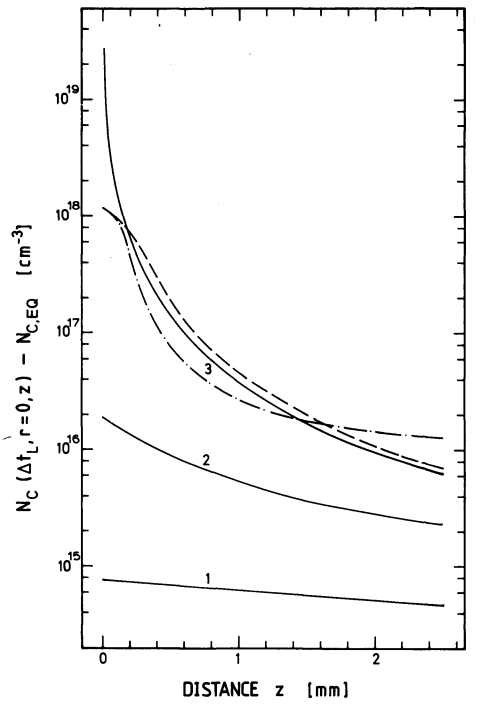

Figure 18 Influence of EL2 absorption dynamics on excess free-electron number density distribution, $N_C(t' = \Delta t_L, r = 0, z) - N_{C,EQ}$. $l = 2.5$ mm, $\theta = 103$ K. Solid curves: $A_L = A_F = 0$ with (1) $I_{0L} = 3 \times 10^7\,W/cm^2$, (2) $I_{0L} = 3 \times 10^8\,W/cm^2$, (3): $I_{0L} = 10^{10}\,W/cm^2$. Dashed curve: $A_L = 3 \times 10^{-35}\,cm^5$, $A_F = 0$, $I_{0L} = 10^{10}\,W/cm^2$. Dash-dotted curve: $A_L = 3 \times 10^{-35}\,cm^5$, $A_F = 10^{-33}\,cm^5$, $I_{0L} = 10^{10}\,W/cm^2$.

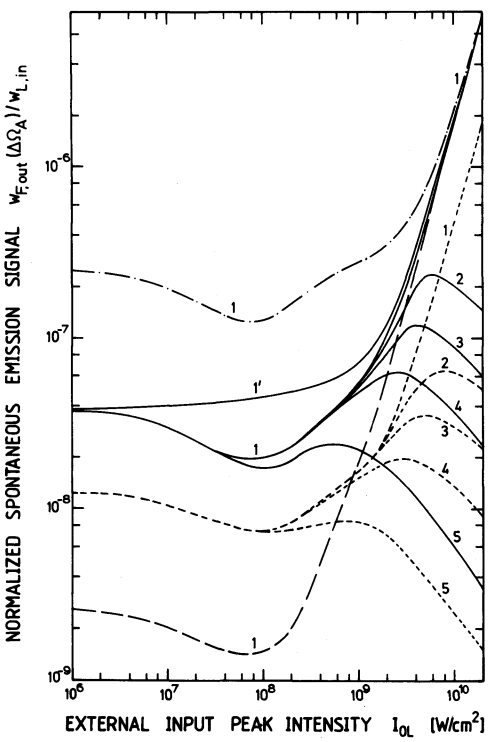

Figure 19 Simulation of experimental spontaneous emission. $l = 2.5$ mm. $A_F = 0$. (——) $N_{C,EQ} = 1.5 \times 10^{17}\,cm^{-3}$, (— —) $N_{C,EQ} = 10^{16}\,cm^{-3}$, and (—·—) $N_{C,EQ} = 10^{18}\,cm^{-3}$ are for $\theta = 103$ K. (– – –) $\theta = 295$ K and $N_{C,EQ} = 1.5 \times 10^{17}\,cm^{-3}$. The parameters of Table I apply except (1) $A_L = 0$; (1') $A_L = 0$ and $k_{CI} = 0$; (2) $A_L = 10^{-35}\,cm^5$; (3) $A_L = 3 \times 10^{-35}\,cm^5$; (4) $A_L = 10^{-34}\,cm^5$; (5) $A_L = 10^{-33}\,cm^5$. A normalized signal of $w_{F,out}(\Delta\Omega_A)/w_{L,in} = \int_{-\infty}^{\infty} I_{F,out}(t', \Delta\Omega_A)\,dt' / \int_{-\infty}^{\infty} I_{L,in}(t')\,dt' = 10^{-6}$ corresponds to an internal fluorescence quantum efficiency of $\eta_{int} \approx 7 \times 10^{-3}$ (see Fig. 11). $\Delta\Omega_A = 0.049$ sr.

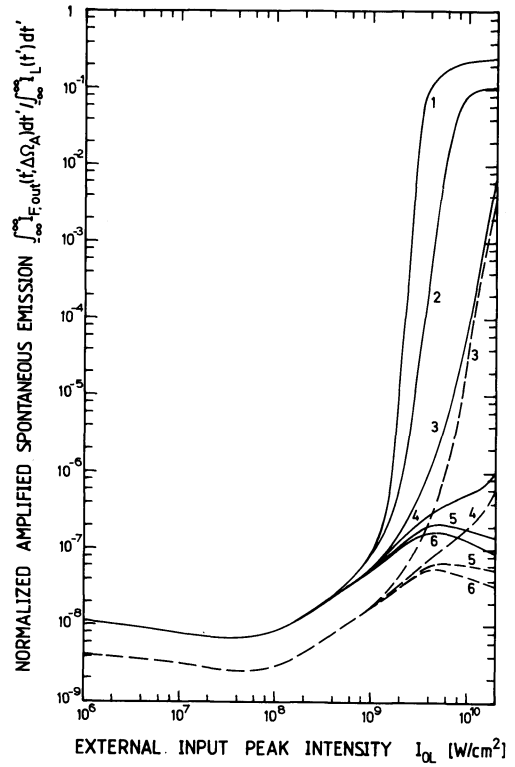

Figure 20 Simulation of experimental amplified spontaneous emission. $l = 0.5$ mm. (——) $\theta = 103$ K, (— —) $\theta = 295$ K. The parameters of Table I apply except (1) $A_L = 0$ and $A_F = 10^{-33}$ cm^5; (2 to 6) $A_L = 3 \times 10^{-35}$ cm^5 with $A_F = 10^{-33}$ cm^5 (2), 3×10^{-34} cm^5 (3), 10^{-34} cm^5 (4), 3×10^{-35} cm^5 (5) and 0 (6).

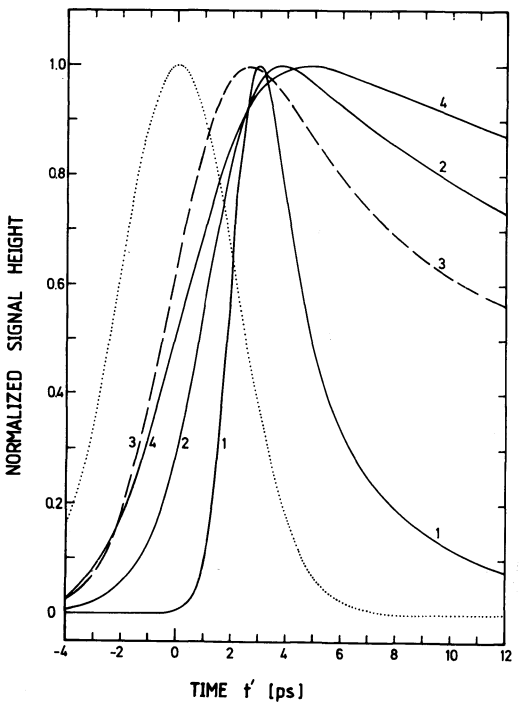

Figure 21 Simulation of emission pulse shapes. $l = 0.5$ mm, $\theta = 103$ K. (· · · ·) Input pump pulse shape. The other curves are calculated applying the parameters of Table I. The pump pulse peak intensity is varied according to $I_{0L} = 3 \times 10^9$ W cm^{-2} (1); 10^9 W cm^{-2} (2); 10^8 W cm^{-2} (3); and 10^6 W cm^{-2} (4).

single-photon absorption of deep-level centres was included. The detailed analysis indicates that for the investigated GaAs crystal the deep-level centre absorption dynamics, the stimulated emission at the pump laser frequency and the longitudinal amplification of spontaneous emission have practically no influence on the energy transmission and the two-photon absorption coefficient. The free-carrier absorption cross-section at the pump laser frequency ν_L is small and therefore has no influence ($A_L N_V - \sigma_{FC}$ is the relevant cross-section).

At high pump pulse intensities the longitudinal amplified spontaneous emission signal in forward direction was found to be limited to $W_{F,out}(\Delta\Omega_A)/W_{L,in} \simeq 10^{-4}$ at a temperature of 103 K. The conversion efficiency is limited probably by the short penetration depth of the pump laser at high pump pulse intensities which favours amplified spontaneous emission into all directions or into transverse directions. The feed-back of fluorescence light (laser oscillation) gave energy conversion efficiencies up to 2×10^{-3} ($\vartheta = 103\,\mathrm{K}$, $l = 0.5\,\mathrm{mm}$). Improved feedback (the exit surface of 0.5 mm crystal was only roughly polished) by better surface polishing and mirror coating should increase the conversion efficiency further.

References

1. N. G. BASOV, A. Z. GRASYUK, I. G. ZUBAREV, V. A. KATULIN and O. N. KROKHIN, *Soviet Phys. JETP* **23** (1966) 366.
2. V. V. ARSEN'EV, V. S. DNEPROVSKII, D. N. KLYSHKO and A. N. PENIN, *ibid.* **29** (1969) 413.
3. J. M. RALSTON and R. K. CHANG, *Appl. Phys. Lett.* **15** (1969) 164.
4. YA. A. OKSMAN, A. A. SEMENOV, V. N. SMIRNOV and O. M. SMIRNOV, *Soviet Phys. Semicond.* **6** (1972) 629.
5. D. A. KLEINMAN, R. C. MILLER and W. A. NORDLAND, *Appl. Phys. Lett.* **23** (1973) 243.
6. A. Z. GRASIUK, I. G. ZUBAREV, V. V. KOBKO, YU. A. MATVEETS, A. B. MIRONOV and O. B. SHATBERASHVILI, *JETP Lett.* **17** (1973) 416.
7. C. C. LEE and H. Y. FAN, *Phys. Rev.* **B9** (1974) 3502.
8. S. J. BEPKO, *ibid.* **B12** (1975) 669.
9. J. H. BECHTEL and W. L. SMITH, *ibid.* **B13** (1976) 3515.
10. H. LOTEM, J. H. BECHTEL and W. L. SMITH, *Appl. Phys. Lett.* **28** (1976) 389.
11. I. G. ZUBAREV, A. B. MIRONOV and S. J. MIKHAILOV, *Soviet Phys. Semicond.* **11** (1977) 239.
12. B. BOSACCHI, J. S. BESSEY and F. C. JAIN, *J. Appl. Phys.* **49** (1978) 4609.
13. A. F. STEWART and M. BASS, *Appl. Phys. Lett.* **37** (1980) 1040.
14. T. F. BOGGESS, A. L. SMIRL, S. C. MOSS, I. W. BOYD and E. W. VAN STRYLAND, *IEEE J. Quantum Electron.* **QE-21** (1985) 488.
15. A. L. SMIRL, T. F. BOGGESS, S. C. MOSS and I. W. BOYD, *J. Luminesc.* **30** (1985) 272.
16. E. W. VAN STRYLAND, H. VANHERZEELE, M. A. WOODALL, M. J. SOILEAU, A. L. SMIRL, S. GUHA and T. F. BOGGESS, *Opt. Engng* **24** (1985) 613.
17. A. SAISSY, A. AZEMA, J. BOTINEAU and F. GIRES, *Appl. Phys.* **15** (1978) 99.
18. S. JAYARAMAN and C. H. LEE, *Appl. Phys. Lett.* **20** (1972) 392.
19. M. GERSHENZON, 'Semiconductors and Semimetals', Vol. 2: 'Physics of III–V Components', edited by R. K. Willardson and A. C. Beer (Academic Press, New York, 1966) p. 289.
20. E. W. WILLIAMS and H. B. BEBB, *ibid.*, Vol. 8: 'Transport and Optical Properties', edited by R. K. Willardson and A. C. Beer (Academic Press, New York, 1972) p. 321.
21. Y. P. VARSHIN, *Phys. Status Solidi* **20** (1967) 9.
22. J. I. PANKOVE, 'Optical Processes in Semiconductors' (Dover, New York, 1971).
23. S. TANAKA, H. SAITO, H. YOSHIDA and S. SHIONOYA, 'Semiconductors Probed by Ultrafast Laser Spectroscopy', Vol. 1, edited by R. R. Alfano (Academic Press, Orlando, 1984) p. 171.
24. D. R. WRIGHT, 'Gallium Arsenide', edited by M. J. Howes and D. V. Morgan (Wiley, Chichester, 1985) p. 1.
25. P. D. DAPKUS, N. HOLONYAK, JR, R. D. BURNHAM, D. L. KEUNE, J. W. BURD, K. L. LAWLEY and R. E. WALLINE, *J. Appl. Phys.* **41** (1970) 4194.
26. S. TANAKA, H. KOBAYASHI, H. SAITO and S. SHINOYA, *J. Phys. Soc. Jpn* **49** (1980) 1051.

27. W. L. CAO, A. M. VAUCHER and C. H. LEE, *Appl. Phys. Lett.* **38** (1981) 306.
28. N. G. BASOV, A. Z. GRASYUK, I. G. ZUBAREV and V. A. KATULIN, *JETP Lett.* **1** (1965) 118.
29. W. L. CAO, A. M. VAUCHER and C. H. LEE, *Appl. Phys. Lett.* **38** (1981) 653.
30. D. V. LANG and R. A. LOGAN, *J. Electron. Mater.* **4** (1975) 1053.
31. G. M. MARTIN, A. MITONNEAU and A. MIRCEA, *Electron. Lett.* **13** (1977) 191.
32. A. MITTONNEAU and A. MIRCEA, *Solid St. Commun.* **30** (1979) 157.
33. A. CHANTRE, D. BOIS and G. VINCENT, *Phys. Rev.* **B23** (1981) 5335.
34. G. VINCENT, D. BOIS and A. CHANTRE, *J. Appl. Phys.* **53** (1982) 3643.
35. M. KAMINSKA, M. SKOWRONSKI, J. LAGOWSKI, J. M. PARSEY and H. C. GATOS, *Appl. Phys. Lett.* **43** (1983) 302.
36. P. DOBRILLA and J. S. BLAKEMORE, *J. Appl. Phys.* **58** (1985) 208.
37. G. M. MARTIN and S. MAKRAM-EBEID, 'Deep Centers in Semiconductors, A State-of-the-Art-Approach', edited by S. T. Pantelides (Gordon and Breach, New York, 1986) Ch. 6.
38. A. L. SMIRL, G. C. VALLEY, K. M. BOHNERT and T. F. BOGGESS, *IEEE J. Quantum Electron.* **QE-24** (1988) 289.
39. G. C. VALLEY and A. L. SMIRL, *ibid.* **QE-24** (1988) 304.
40. K. ISHIDA, A. YAHATA and T. KIKUTA, *Jpn J. Appl. Phys.* **24** (1985) L250.
41. P. SILVERBERG, P. OMLING and L. SAMUELSON, *Appl. Phys. Lett.* **52** (1988) 1689.
42. D. T. F. MARPLE, *J. Appl. Phys.* **35** (1964) 1241.
43. B. O. SERAPHIN and H. E. BENNETT, 'Semiconductors and Semimetals', Vol. 3: 'Optical Properties of III–V Compounds', edited by R. K. Willardson and A. C. Beer (Academic Press, New York, 1967) p. 513.
44. J. S. BLAKEMORE, *J. Appl. Phys.* **53** (1982) R123.
45. A. PENZKOFER, D. VON DER LINDE and A. LAUBEREAU, *Opt. Commun.* **4** (1972) 377.
46. H. J. EICHLER, P. GÜNTER and D. W. POHL, 'Laser-induced Dynamic Gratings', (Springer-Verlag, Berlin, 1986). (Springer Series in Optical Sciences, Vol. 50.)
47. C. V. SHANK and D. H. AUSTON, *Phys. Rev. Lett.* **34** (1975) 479.
48. A. PENZKOFER and W. LEUPACHER, *J. Luminescence* **37** (1987) 61.
49. W. VAN ROOSBROECK and W. SHOCKLEY, *Phys. Rev.* **94** (1954) 1558.
50. M. D. STRUGE, *ibid.* **127** (1962) 768.
51. G. M. MARTIN, 'Proceedings of the First International Conference on Semi-insulating III–V Material', edited by E. J. Rees (Shiva, Nantwich, 1980) p. 13.
52. C. J. HWANG, *J. Appl. Phys.* **40** (1969) 4584.
53. D. E. HILL, *Phys. Rev.* **133A** (1964) 866.
54. H. J. QUEISSER and C. S. FULLER, *J. Appl. Phys.* **37** (1966) 4895.
55. E. W. WILLIAMS, *Phys. Rev.* **168** (1968) 922.
56. H. B. BEBB and E. W. WILLIAMS, 'Semiconductors and Semimetals', Vol. 8: 'Transport and Optical Phenomena', edited by R. K. Willardson and A. C. Beer (Academic Press, New York, 1972) p. 181.
57. A. VON LEHMEN and J. M. BULLANTYNE, *J. Appl. Phys.* **58** (1985) 958.
58. P. SPERBER and A. PENZKOFER, *Opt. Quantum Electron.* **18** (1986) 381.
59. A. PENZKOFER and W. LEUPACHER, *ibid.* **19** (1987) 327.
60. P. SPERBER, W. SPANGLER, B. MEIER and A. PENZKOFER, *ibid.* **20** (1988) 395.
61. P. QIU and A. PENZKOFER, *Appl. Phys.* **B48** (1989) 115.
62. H. J. POLLARD, T. ELSAESSER, A. SEILMEIER and W. KAISER, *Appl. Phys.* **B32** (1983) 53.
63. ZS. BOR, S. SZATMARI and A. MÜLLER, *Appl. Phys.* **B32** (1983) 101.
64. A. PENZKOFER, *Appl. Phys.* **B40** (1986) 85.
65. W. G. SPITZER and J. M. WHELAN, *Phys. Rev.* **114** (1959) 59.